MIT Open Access Articles

Grain Boundary Engineering for Improved Thin Silicon Photovoltaics

The MIT Faculty has made this article openly available. ***Please share*** how this access benefits you. Your story matters.

Citation	Raghunathan, Rajamani, Eric Johlin, and Jeffrey C. Grossman. "Grain Boundary Engineering for Improved Thin Silicon Photovoltaics." Nano Lett. 14, no. 9 (September 10, 2014): 4943–4950.
As Published	http://dx.doi.org/10.1021/nl501020q
Publisher	American Chemical Society (ACS)
Version	Author's final manuscript
Citable link	http://hdl.handle.net/1721.1/101939
Terms of Use	Article is made available in accordance with the publisher's policy and may be subject to US copyright law. Please refer to the publisher's site for terms of use.

Massachusetts Institute of Technology

DSpace@MIT

NANO LETTERS

Access provided by MIT Libraries

Subscriber access provided by MIT Libraries

Communication

Grain Boundary Engineering for Improved Thin Silicon Photovoltaics

Rajamani Raghunathan, Eric C. Johlin, and Jeffrey C. Grossman

Nano Lett., **Just Accepted Manuscript** • DOI: 10.1021/nl501020q • Publication Date (Web): 25 Jun 2014

Downloaded from http://pubs.acs.org on August 15, 2014

Just Accepted

"Just Accepted" manuscripts have been peer-reviewed and accepted for publication. They are posted online prior to technical editing, formatting for publication and author proofing. The American Chemical Society provides "Just Accepted" as a free service to the research community to expedite the dissemination of scientific material as soon as possible after acceptance. "Just Accepted" manuscripts appear in full in PDF format accompanied by an HTML abstract. "Just Accepted" manuscripts have been fully peer reviewed, but should not be considered the official version of record. They are accessible to all readers and citable by the Digital Object Identifier (DOI®). "Just Accepted" is an optional service offered to authors. Therefore, the "Just Accepted" Web site may not include all articles that will be published in the journal. After a manuscript is technically edited and formatted, it will be removed from the "Just Accepted" Web site and published as an ASAP article. Note that technical editing may introduce minor changes to the manuscript text and/or graphics which could affect content, and all legal disclaimers and ethical guidelines that apply to the journal pertain. ACS cannot be held responsible for errors or consequences arising from the use of information contained in these "Just Accepted" manuscripts.

ACS Publications
High quality. High impact.

Nano Letters is published by the American Chemical Society. 1155 Sixteenth Street N.W., Washington, DC 20036
Published by American Chemical Society. Copyright © American Chemical Society. However, no copyright claim is made to original U.S. Government works, or works produced by employees of any Commonwealth realm Crown government in the course of their duties.

1
2
3
4
5
6
7
8
9
10
11
12
13
14
15
16
17
18
19
20
21
22
23
24
25
26
27
28
29
30
31
32
33
34
35
36
37
38
39
40
41
42
43
44
45
46
47
48
49
50
51
52
53
54
55
56
57
58
59
60

Grain Boundary Engineering for Improved Thin Silicon Photovoltaics

Rajamani Raghunathan,[†] Eric Johlin,[‡] and Jeffrey C. Grossman[*,†]

Department of Materials Science and Engineering, Massachusetts Institute of Technology, 77 Massachusetts Avenue, Cambridge, MA 02139, and Department of Mechanical Engineering, Massachusetts Institute of Technology, 77 Massachusetts Avenue, Cambridge, MA 02139.

E-mail: jcg@mit.edu

KEYWORDS: Photovoltaics, Grain boundary engineering, Density functional theory, Silicon

Abstract

In photovoltaic devices, the bulk disorder introduced by grain boundaries (GBs) in polycrystalline silicon is generally considered to be detrimental to the physical stability and electronic transport of the bulk material. However, at the extremum of disorder, amorphous silicon is known to have a beneficially increased band gap, and enhanced optical absorption. This study is focused on understanding and utilizing the nature of the most commonly encountered Σ_3 GBs, to balance the incorporation the advantageous properties of amorphous silicon, while avoiding the degraded electronic transport

[*]To whom correspondence should be addressed

[†]Department of Materials Science and Engineering, Massachusetts Institute of Technology, 77 Massachusetts Avenue, Cambridge, MA 02139

[‡]Department of Mechanical Engineering, Massachusetts Institute of Technology, 77 Massachusetts Avenue, Cambridge, MA 02139.

1
2
3
4
5
6
7
8
9
10
11
12
13
14
15
16
17
18
19
20
21
22
23
24
25
26
27
28
29
30
31
32
33
34
35
36
37
38
39
40
41
42
43
44
45
46
47
48
49
50
51
52
53
54
55
56
57
58
59
60

of a fully amorphous system. A combination of theoretical methods is employed to understand the impact of Σ_3 GBs on the materials properties and full-device photovoltaic performance.

Introduction

In 2012, crystalline (c-Si) silicon composed the active layer of 89% of photovoltaic (PV) modules produced worldwide, with thin film (generally amorphous) silicon (a-Si:H) accounting for an additional 4%.[1] As is well established, while the electron and hole mobilities of c-Si are quite high, the material suffers from poor optical absorption, and a sub-optimal, indirect band gap. In a-Si:H, the situation is reversed - the optical absorption is significantly increased relative to c-Si due to its direct bandgap, and the theoretical efficiency improved from the shift toward the optimal 1.34 eV gap,[2] but the low hole mobility limits the cell performance.[3] Additionally, the Stabler-Wronski effect, a light-induced degradation mechanism, reduces cell efficiencies further, by 10% to 30% within few days of sun exposure.[4,5] Nano-(and micro-)crystalline silicon (both referred to as nc-Si here, for simplicity) attempt to strike a beneficial balance between amorphous and crystalline silicon, maintaining most of the increased absorption and band gap of the a-Si:H,[6] while improving upon the carrier mobilities toward those of c-Si.[7] Despite the potential of such an approach, nc-Si device efficiencies still remain below those of either a-Si:H or c-Si.[8] While nc-Si represents an attempt to move the deficient properties of a-Si toward those of c-Si, the limited performance of the material along with the fact that the best nc-Si devices occur at low crystalline volume fractions indicate that this approach may not be feasible.[9–11] In contrast to the case of nc-Si, where order is introduced into a disordered material, the opposite approach, namely introduction of disorder into an otherwise-crystalline material, has received far less attention. One possibility for doing this would be to leverage the diversity of GB orientations and misfit angles already present in polycrystalline materials. For this to be successful, however, it would be necessary to achieve an improved absorption and bandgap (toward those of a-Si:H)

1
2
3
4
5
6
7
8
9
10
11
12
13
14
15
16
17
18
19
20
21
22
23
24
25
26
27
28
29
30
31
32
33
34
35
36
37
38
39
40
41
42
43
44
45
46
47
48
49
50
51
52
53
54
55
56
57
58
59
60

without substantial degradation the superior transport properties of c-Si, and demonstrate that these properties combined into full device-scale PV efficiency improvements.

Of the numerous types of GBs possible in a polycrystalline material, experiments and theoretical models show that Σ_3, Σ_9 and Σ_{27} GBs are energetically favored in polycrystalline silicon; in particular Σ_3 GBs are most frequently encountered.[12,13] Thanks to the recent advancements in grain boundary engineering (GBE) and high resolution transmission electron microscopy (HRTEM), it is now possible to incorporate GBs with a specific character into a material.[14–16] This has led to numerous studies related to the energetics, atomic and electronic structure and defect physics in semiconductor GBs, with emphasis on understanding the impact of these properties on electronic transport.[17–22] However, in order to answer the question of whether GBE could be beneficial to PV, both the electronic and optical properties must be understood, and simultaneously optimized.

In this work, density functional theory (DFT) is employed to characterize Σ_3 coincidence site lattice GBs in silicon and to predict which of these GBs may be beneficial to solar energy conversion. Using our computed band structures and optical absorption coefficients we show that, depending on the interface atomic structure, particular GBs can exhibit either significantly higher or lower optical absorption relative to c-Si throughout the visible spectrum, as well as modified band gaps. We further compute the electronic conductivities, σ, using a Boltzmann transport approach to assess the impact of such GBs on charge transport. These results are combined into a finite element model to predict energy conversion efficiencies of GBE solar cells, where it is shown that significant enhancements in energy conversion efficiency over c-Si may be possible for thin device configurations.

Methodology

The starting Σ_3 GB structures were obtained using the *GB Studio* program.[23] The coincidence site lattice GB structures consist of two crystal-like regions or grains (A and B),

1
2
3
4
5
6
7
8
9
10
11
12
13
14
15
16
17
18
19
20
21
22
23
24
25
26
27
28
29
30
31
32
33
34
35
36
37
38
39
40
41
42
43
44
45
46
47
48
49
50
51
52
53
54
55
56
57
58
59
60

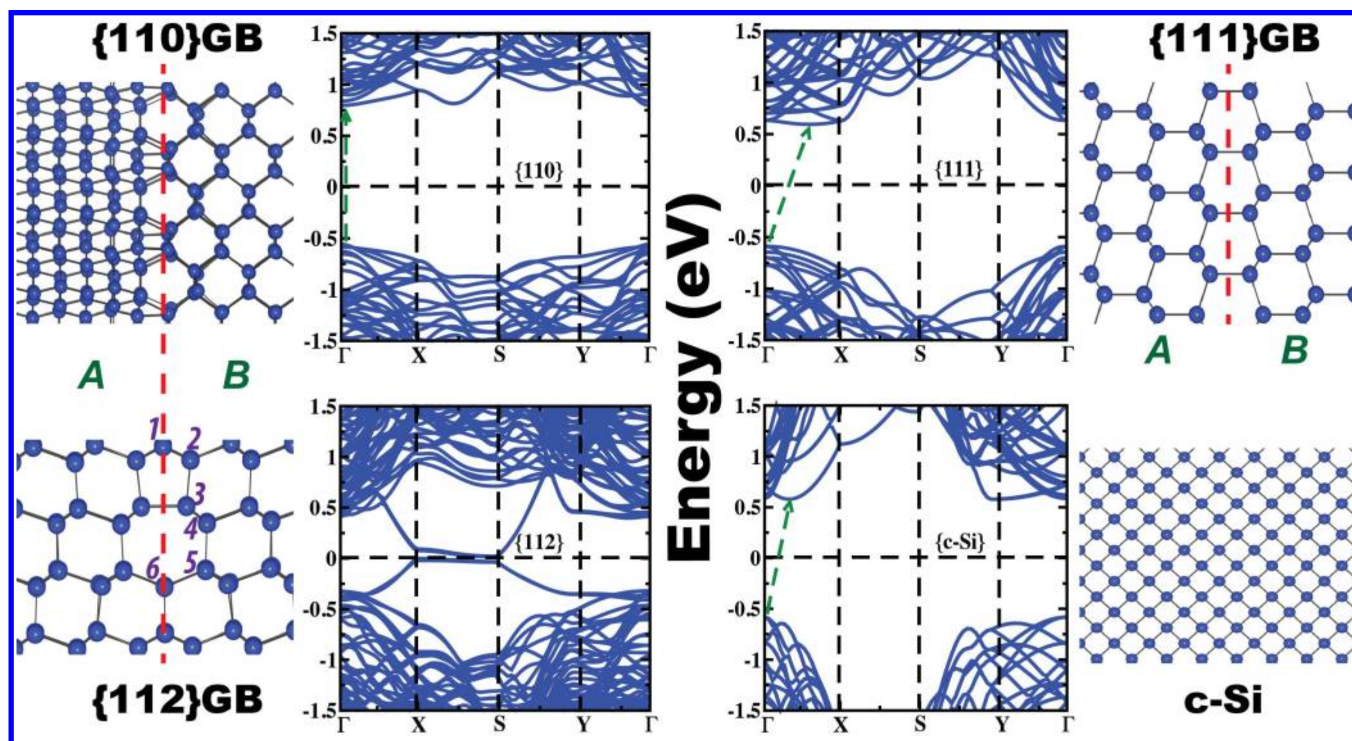

Figure 1: Atomic and electronic structures of (top-left) {110}, (top-right) {111}, (bottom-left) {112} GBs, and (bottom-right) c-Si. The GB interfaces are marked by dashed lines. The regions marked A and B form the crystalline regions or grains. In the band structure plots the Fermi energy is at zero and the dashed green lines indicate the band gap.

1
2
3
4
5
6
7
8
9
10
11
12
13
14
15
16
17
18
19
20
21
22
23
24
25
26
27
28
29
30
31
32
33
34
35
36
37
38
39
40
41
42
43
44
45
46
47
48
49
50
51
52
53
54
55
56
57
58
59
60

which form an interface along a chosen crystallographic plane, {110}, {111} or {112} (see Fig. 1). The grains A and B are misoriented with respect to one another by an angle Ω, either parallel to the GB interface (as in the {111} and {112} tilt GBs), or perpendicular to the GB surface (as in the {110} twist boundary). The tetragonal supercell was repeated in all three directions using periodic boundary conditions (PBC). Each supercell contains two GBs, one in the middle of the supercell and the other due to the PBC along the direction normal to the GB plane.

First-principles calculations were performed within the framework of DFT using the Vienna ab-initio simulation program.[24] The projector-augmented wave method with the generalized gradient approximation PBE (GGA-PBE) was used for the exchange-correlation potential.[25–28] A plane wave basis cutoff energy of 350 eV and well converged k-point mesh of $(4 \times 4 \times 4)$ were used in all calculations. All structures were allowed to relax until the forces acting on each atom were less than 0.01 eV/Å. The fully relaxed structures were used to compute the electronic band structure. In order to gain a qualitative understanding of optical absorption of GBE materials the absorption coefficients were computed from the imaginary part of dielectric constants computed from DFT within the random phase approximation. The room temperature (300K) electronic conductivities for n and p type structures were computed by employing the Boltzmann transport equation within the constant relaxation time approximation using the energy eigenvalues obtained from DFT, as this approach is known to accurately describe the electronic properties of metals and semiconductors.[29–34] In order to obtain converged results we used a dense k-point mesh containing 68 points in the irreducible Brillouin zone. The principal components of electronic conductivity, σ_x, σ_y and σ_z, were obtained by diagonalizing the conductivity tensor Σ computed from the relation

$$\Sigma = e^2 \tau \sum_n \int \frac{d\mathbf{k}}{4\pi^3} \left(-\frac{\partial f(\epsilon_{nk})}{\partial \epsilon_{nk}} \right) \mathbf{v}_{nk} \mathbf{v}_{nk} \quad (1)$$

where e is the electronic charge, τ is the relaxation time, $\mathbf{k}$ is the reciprocal lattice vector,

1
2
3
4
5
6
7
8
9
10
11
12
13
14
15
16
17
18
19
20
21
22
23
24
25
26
27
28
29
30
31
32
33
34
35
36
37
38
39
40
41
42
43
44
45
46
47
48
49
50
51
52
53
54
55
56
57
58
59
60

ϵ_{nk} is the energy eigenvalue of nth band at $\mathbf{k}$ (DFT eigenvalues), $f(\epsilon_{nk})$ Fermi-Dirac function at temperature T, and $\mathbf{v}_{nk} = (1/\hbar)\nabla_k \epsilon_{nk}$.[35] The value of τ was chosen based on previous far-infrared reflectance spectra studies on phosphorus doped silicon in the concentration range $10^{17} - 10^{18} cm^{-3}$.[36] We further confirmed that the computed conductivity values for c-Si matches well with that reported by Weber et. al.[37] The same relaxation time was used in our calculations for {110} and {111} GBs as well. This is reasonable since, our computed charge density of valance and conduction bands showed "bulk" like character and we do not expect any recombination centers. Another factor relevant to this discussion is the scattering by phonons at the interface which is not included in this present study. We assume that this is small since we are using GBs with high symmetry like the Σ_3 GB. Finite-element device modeling was performed using *COMSOL* with light absorption and carrier generation simulated by solving the Helmholtz wave-optics equation and the diffusion of charged species in the material modeled using a drift-diffusion model. More details about the methodology can be found in the supplementary information.

Atomic Structure

The grain boundary formation energies (E_{GB}) for the relaxed structures were obtained using $E_{GB} = (E_{GBS} - E_{Bulk})/2S$, where E_{GBS} is the energy of the relaxed structure with a GB, E_{Bulk} is the energy of bulk c-Si with no GBs, but containing the same number of Si atoms, S is the GB surface area, and the factor of 2 comes from the supercell containing two grain boundaries. The number of unit cells inside grains A and B along the direction normal to the GB plane was increased until the E_{GB} values were converged to less than 10^{-3}eV/Å^2, in order to eliminate any interaction between the neighboring GBs. Convergence was achieved for structures with separation between the neighboring GBs greater than 3nm. The GB energies showed that {111} ($E_{GB} = 0.001$ eV/Å^2) is the most favorable GB, with negligible deviation from the ideal silicon tetrahedral structure. The GB energies for {110} and {112}

structures were found to be 0.040eV/Å^2 and 0.042 eV/Å^2 respectively, suggesting extensive rearrangement of atoms at the interface. This was further confirmed from the calculated bond length and bond angle distributions in the relaxed structures which showed that the {112} GB cores contain highly strained bonds (see supplementary information). In addition, the {112} GB also contains 5-fold coordinated silicon atoms, indexed by "1", as shown in Fig. 1. The fact that we observe these coordination defects at the disordered grain boundaries is not entirely surprising, as floating bonds are known to occur in a-Si:H structures. The 5-fold coordinated atoms in the {112} GB are associated with four highly strained bonds of length $\approx$ 2.55Å(corresponding to 8% increase over ideal Si-Si bond length), and a fifth unstrained bond of length 2.37Å. Thus, we expect defect levels highly localized around the dislocation core in the electronic structure of a {112} GB. While such strained bonds are completely absent in the {111} GB, the {110} structure possesses a small number of bonds with less than 3% compressive strain. Neither {111} nor {110} GB however show any under- or over-coordinated silicon atoms. The relaxed GB structures as well as the computed GB energies are consistent with previously reported GB structures using HRTEM results and DFT.[38,39]

Electronic Band Structure

As mentioned, our GB structures contain multiple unit cells in each direction in order to describe the GB interface adequately and also to avoid direct interaction between the neighboring GBs. Such periodic supercell treatments can often lead to folding of energy bands though they do not alter the fundamental energy gap (a more detailed description of zone folding can be found in the SI). Zone folding pose a challenge to the analysis of the electronic structures of extended supercells and has already been previously reported in {110} oriented semiconducting nanostructures such as silicon and germanium nanotubes, nanowires, and quantum slabs.[40–44] Though the unfolded band structure can be reconstructed from zone-

1 2 3 4 5 6 7 8 9 10 11 12 13 14 15 16 17 18 19 20 21 22 23 24 25 26 27 28 29 30 31 32 33 34 35 36 37 38 39 40 41 42 43 44 45 46 47 48 49 50 51 52 53 54 55 56 57 58 59 60

folded band structures, the goal of this work is to understand the fundamental energy gaps in GB engineered structures,[45,46] and thus such reconstruction is not considered here.

The GGA-PBE band structures of GB structures along different symmetry directions in a tetragonal Brillouin zone are shown in Fig. 1, together with that of a single-crystal silicon supercell containing the same number of atoms for comparison. The conduction bands of the semiconducting structures, namely the {110} and {111} GBs, and c-Si, are scissor-shifted by 0.57eV to match the experimental band gap E_g =1.17eV of c-Si. This correction term is widely employed to account for quasi-particle energy corrections in silicon.[42,47,48] It is however not applied to the {112} GB system since it shows metallic behavior unlike the {110} and {111} GBs in which the valence and conduction band edges have bulk like character. We emphasize here that the band structure of c-Si presented in the figure is that of an extended supercell of silicon and *not* of a primitive unit cell calculation. The periodic nature of the supercell produces a large number of shallow and flat bands in these extended structures due to zone-folding (refer SI for a details). The calculated band gaps for the {110} GB, {111} GB, and single-crystal structures are 1.38 eV, 1.22 eV, and 1.17 eV, respectively. As expected, our calculated band structure for the {112} GB showed deep defect levels throughout the entire gap, giving rise to a semi-metallic density of states with a small overlap between the occupied and unoccupied bands at the fermi level, similar to that observed in high pressure phases of silicon such as BC8, and is attributed to the presence of structural deformations caused by coordination defects.[48,49] In order to further substantiate the metallic nature of the {112} GB, we computed the energy gaps of all the GB structures using the modified Becke-Johnson[50] meta-GGA functional which is known to predict the band gaps of a wide range of elemental and compound semiconductors accurately with reasonable computational effort compared to hybrid functionals and GW calculations. The meta-GGA gaps are in good agreement with the scissor corrected PBE results for the semiconducting structures as well as it predicted {112} GB to be semi-metallic in line with GGA-PBE. Analysis of the valence and conduction band charge densities for the {112} GB

ACS Paragon Plus Environment

1
2
3
4
5
6
7
8
9
10
11
12
13
14
15
16
17
18
19
20
21
22
23
24
25
26
27
28
29
30
31
32
33
34
35
36
37
38
39
40
41
42
43
44
45
46
47
48
49
50
51
52
53
54
55
56
57
58
59
60

further confirm that the charge density is highly localized near the strained bonds of the 5-fold coordinated silicon atoms (see supplementary information). The computed valence and conduction band charge densities for the {110} and {111} GB cases, show delocalization across the entire supercell similar to that found in crystalline silicon. As it is well known in literature that point defects are highly concentrated in the GB core, we performed DFT calculations with vacancy defects in the bulk region as well as in the GBs to understand its effect on the electronic structure.[51] Using charge densities computed within the GGA approximation in DFT, we find that while a Si vacancy in {112} GBs can remove deep level states in the energy gap formed by the otherwise-present floating bonds, vacancies create defect states in {110} GB[38] (see Supplementary information). The vacancies in {110} GBs, however, produce shallow defect states close to the valance and conduction bands, which are far less detrimental to lifetime than the mid-gap states found in {112} GBs. We furthermore computed the formation energies for various locations of vacancy defects in {110} and {112} GBs relative to a vacancy defect in bulk region and found that the GBs are more favorable for defect formation compared to the grain bulk. The lowest defect formation energy in {112} GB (-3.13eV) is about 2 times lower than that in {110} GB (-1.36eV) suggesting that the {112} GBs are more susceptible for defect formation. Although the presence of defect states is undesirable as these states can act as charge traps and degrade the carrier mobilities, their lower probability of occurring in the crystal core, coupled with our highly-oriented configuration, should decrease the severity of their presence. Furthermore, it could also be possible to passivate these defects by heat-treatment with hydrogen, as shown in previous works.[19,21]

We next computed the dependence of the band gaps (E_g) of the three GB structures as a function of the spacing between them. Our results show a decreasing trend with increasing GB spacing for both the {111} and {110} semiconducting GBs (Fig. 2). The {112} GB showed metallic behavior for all the GB spacings that we studied. The observed E_g behavior is consistent with the computed cohesive energy per atom of GB structures ($E_c(GB)$) with

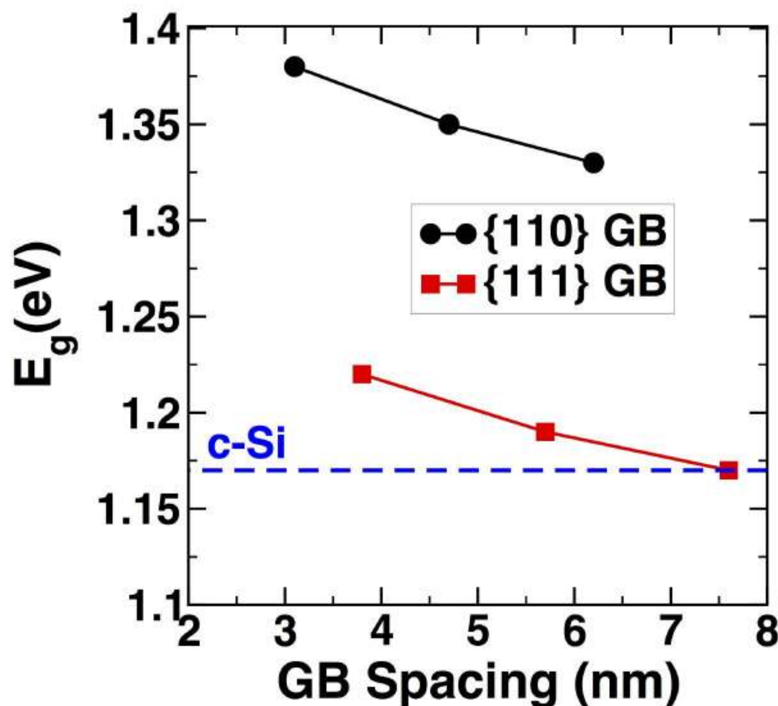

Figure 2: Variation of the energy gap, E_g of semiconducting {110} and {111} GBs as a function of GB spacing. The {112} GB displayed metallic behavior for GB spacing up to 10nm, and is not shown. Also shown is the band gap of single crystal silicon as reference (blue dashed line).

c-Si ($E_c(Si)$) as reference, $\Delta E_c = E_c(GB) - E_c(Si)$ (see supplementary information). Our computed cohesive energy of $E_c(Si)$ =4.54eV/atom for c-Si using GGA-PBE functionals is in good agreement with the literature.[52] As expected, ΔE_c decreases with GB spacing for all cases, although the behavior depends upon the amount of distortion or strain at the interface and how strain field dissipates into the crystalline lattice. As the spacing between the GBs is increased, the number of atoms inside the grains A and B increases while the number of GB atoms remains constant. Consequently, the influence of the GB on the final properties becomes weaker at larger GB spacing, as seen by a monotonic decrease of E_g and is expected to converge to c-Si at much larger GB spacing. Unsurprisingly, similar behavior is observed in the optical and electronic properties which is presented in the following sections.

1
2
3
4
5
6
7
8
9
10
11
12
13
14
15
16
17
18
19
20
21
22
23
24
25
26
27
28
29
30
31
32
33
34
35
36
37
38
39
40
41
42
43
44
45
46
47
48
49
50
51
52
53
54
55
56
57
58
59
60

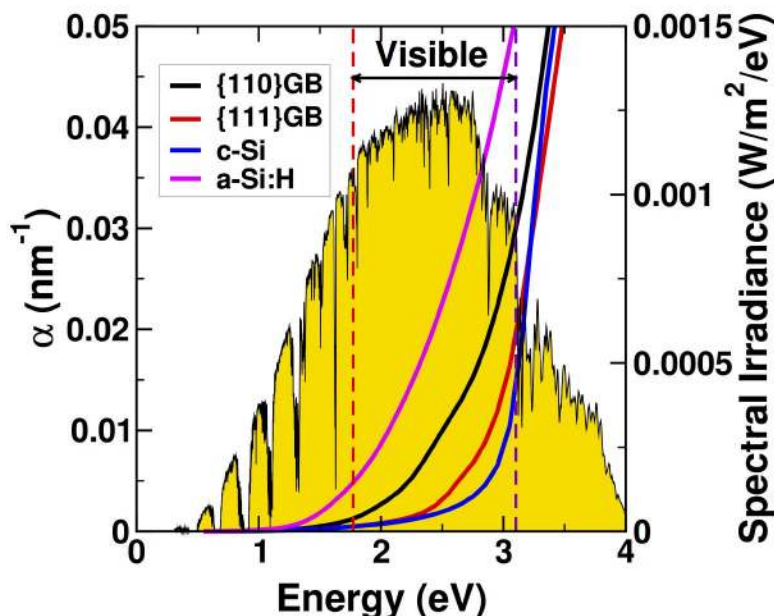

Figure 3: Computed optical absorption coefficient (α) *vs.* energy for two GB structures, and a-Si:H and c-Si for comparison. The AM1.5 solar power spectrum as a function of incident energy is shown as the shaded region.

Optical Properties

As seen in Fig. 2, the band gaps for both the {110} and {111} GBs in silicon are close to the band gap of c-Si, and therefore suitable for efficient PV operation. However, it is crucial to understand the full optical absorption spectrum of these materials in order to predict the performance of GBE structures for PV. In Fig. 3 we show the computed absorption coefficient (α) as a function of excitation energy for the {110} and {111} GBs with 3nm spacing, and c-Si and a-Si:H for comparison. The absorption coefficients of a-Si:H were averaged over 4 snapshots, obtained from the online material of Ref. [53] and relaxed using DFT. Since the {112} GB shows zero band gap, its optical properties were not computed. The computed α values for the {111} structure are quite similar to the case of crystalline silicon, although with a slight enhancement in the blue region of the spectrum. However, the {110} GB shows a significant increase in the optical absorption over much of the visible part of the spectrum. This is because the symmetry breaking at the interface leads to non-zero

1 2 3 4 5 6 7 8 9 10 11 12 13 14 15 16 17 18 19 20 21 22 23 24 25 26 27 28 29 30 31 32 33 34 35 36 37 38 39 40 41 42 43 44 45 46 47 48 49 50 51 52 53 54 55 56 57 58 59 60

transition dipoles between the valence band and interface states located at about 2eV above the valence band. To support this hypothesis, we computed the band decomposed charge densities of bands that are ~2eV above the valence band, since these states show non zero transition dipoles. We found that these optically allowed transitions are localized around the GB core (see supplementary information) and hence can be populated when excited by photons of energy 2eV. We also computed the optical properties of the {110} GB case as a function of spacing between GBs, and found that even at 6.2nm spacing the absorption coefficients are significantly higher than for c-Si in the visible region (see supplementary information). Since solar power is concentrated between 1.0 and 3.8 eV, it is quite beneficial to improve absorption in this energy window, yielding a net 16% relative increase in absorbed photons, and as such, this {110} GB case appears to support our original hypothesis that GBE could be used to enhance the PV performance of silicon solar cells. However, in order to assess the potential of a {110} GB solar cell, we must also determine how the electronic transport is impacted.

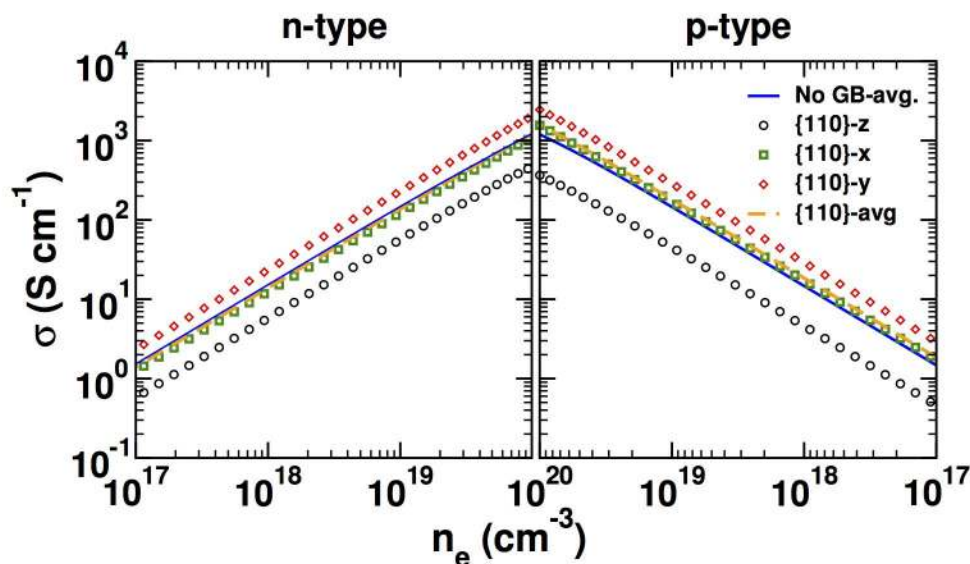

Figure 4: Electronic conductivities of the {110} GB structure with 3nm spacing as a function of dopant concentration (n_e) for both n and p type silicon. For the GB cases the conductivity is shown separately as well as the average value, with the c-Si case shown for comparison.

Electronic Conductivity

The presence of band folding effects in our extended systems makes it difficult to understand the nature of electron and hole mobilities from simply inspecting the curvatures of the band structures. Hence, we explicitly computed the electrical conductivities of n / p type c-Si and {110} GB structures as a function of doping concentration (n_e) in the range 10^{17} to 10^{20} cm^{-3} for $\tau = 3fs$ using the Boltzmann transport equation, as shown in figure 4. The conductivities obtained in our calculations for the single-crystal case compare well with the values previously reported.[54] Our computed conductivities for the {111} GB are almost identical to the single-crystal case, and hence are not shown (see supplementary information). In the case of the {110} GB the interface atomic structure is different from the bulk and as expected, we find strong anisotropy in σ, with the conductivity along the direction normal to the GB plane (the z-axis in our unit cell) significantly lower than the GB in-plane conductivity. For the direction parallel to the GB plane, we predict a slight increase in σ compared to c-Si. Due to the metallic nature over the length scales considered, as with the optical absorption, the electronic conductivity of the {112} GB was not computed.

A possible explanation for the anisotropic nature of σ is the massive symmetry breaking caused due to the introduction of strain at the interface. A recent first principles study on biaxially strained silicon showed that such strain effects can cause changes in the effective mass depending upon the type (compressive/tensile) and magnitude of strain, leading to an increase or decrease in the electronic conductivity.[55] While our {111} GB did not show any significant strain at the interface, the {110} GB was associated with bond length and angle strains. Thus, in order to establish the origin of the anisotropic nature of σ in {110} GB, the electronic conductivity of c-Si in the presence of strain was computed. Under no-strain or in the presence of isotropic strain, the computed σ was isotropic, but under an anisotropic strain we found strong anisotropy in σ (see supplementary information). These results further show that under an anisotropic strain it is possible to observe increase or decrease in σ along a principle direction. In the case of {110} GB, due to the complex

ACS Paragon Plus Environment

nature of interface geometry with wide bond length and angle distributions, it is difficult to decompose the interface strain to obtain its directional components and understand whether a chosen crystallographic direction will have net compressive or tensile strain. It is, however, interesting to note that despite the strong anisotropy, the average conductivity, given by $\sigma = (\sigma_x + \sigma_y + \sigma_z)/3$ is largely unaffected by the presence of the {110} GB when compared to c-Si. This average conductivity is critical for diffusion-dominated cells in which carriers must traverse multiple directions to be collected by front grid or finger contacts, as in most conventional c-Si devices. We emphasize here that the objective of this work is to use these GBs as an effective medium to absorb photons and generate charge carriers, and transport them along the crystalline columns and *not* across the GBs. Such columnar grains in polycrystalline CdTe have been shown to improve solar-cell performance by constraining the hole transport along the crystalline grain bulk to the back contact rather than across the GBs.[56] Hence, the reduction of carrier mobility along the direction normal to GBs is not crucial for the functioning of GBE devices. We also computed the conductivities for both {111} and {110} GBs for different GB spacings (see supplementary information) and found that the average σ converges towards c-Si as the spacing between the GBs is increased.

Table 1: Key results from the solar cell device models shown in Fig. 5 under AM1.5 illumination.

Device	**GB spacing (nm)**	$\mathbf{J_{SC}}$ **(mA/cm²)**	$\mathbf{V_{OC}}$ **(mV)**	**Fill factor (FF)**	**Efficiency** (η)	$\eta/\eta_{\mathbf{c-Si}}$
A	None	30.07	570	0.82	14.05%	1
B	3.1	30.65	780	0.86	20.56%	1.46
C	4.7	30.55	750	0.85	19.48%	1.39
D	6.2	30.50	730	0.85	18.93%	1.35
E	None	16.9	964	0.58	9.45%	0.68

Device Performance

Next, we utilize the results of the electronic and optical properties in full device simulations, performed for four different structures: (A) single-crystal c-Si, ($B - D$) {110} GB

1
2
3
4
5
6
7
8
9
10
11
12
13
14
15
16
17
18
19
20
21
22
23
24
25
26
27
28
29
30
31
32
33
34
35
36
37
38
39
40
41
42
43
44
45
46
47
48
49
50
51
52
53
54
55
56
57
58
59
60

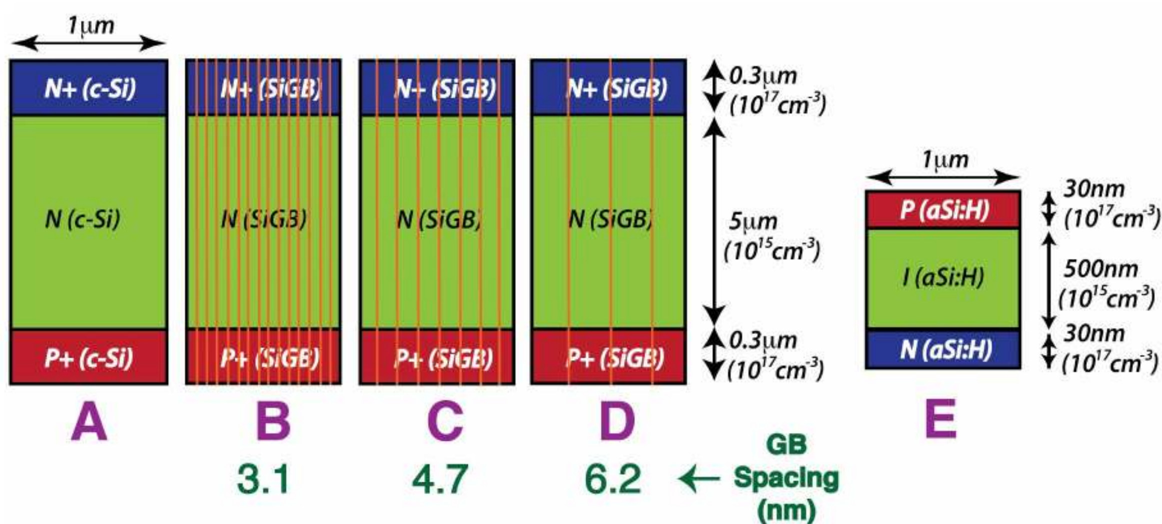

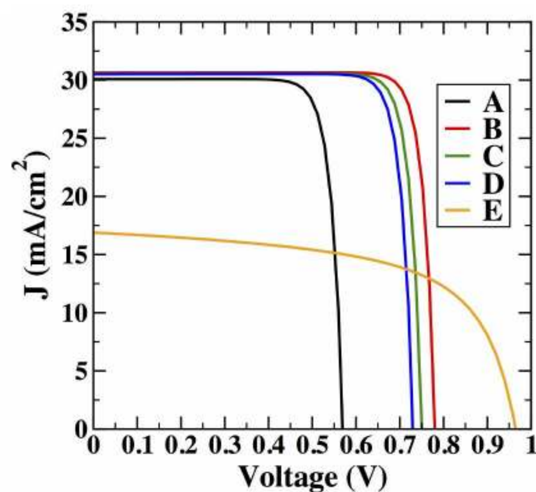

Figure 5: (Top) Schematics of three hypothetical solar cell device configurations. (A) is a reference c-Si device, devices (B-D) contain {110} GBs of spacings between 3.1 and 6.2nm and (E) device with a-Si:H as active material. The layer thickness and the corresponding carrier concentrations (inside brackets) are also shown. (Bottom) Simulated current density (J) *vs.* voltage curves for these four devices.

engineered silicon devices with different GB spacing, and (E) a-Si:H as the active absorber material, schematics of which are shown in Fig. 5 (also see supplementary information). The thickness of devices $(A-D)$ (demarcated in Fig. 5) were chosen to be on the order of those possible through current exfoliation methods,[57] with a constant thickness between these devices employed to demonstrate the influence of the increased absorption of the GBE devices. The thickness of the a-Si:H device (E) was chosen to optimize the device performance, with thicker cells suffering from decreased current collection, and thinner cells from limited absorption, and is included to compare to the fully-disordered silicon limit. The a-Si:H material properties were obtained from.[58] The frequency-dependent dielectric constant obtained from our DFT results were used to compute the complex refractive index and the same was used in our wave optics simulation along with the computed (scissor-shifted) band gaps. We used electron (hole) mobility values of 1450 (450) $cm^2/(V \cdot s)$ for devices $(A-D)$ in our drift-diffusion model, since our electron transport calculations discussed in the previous section did not show any significant degradation in the presence of GBs. For device E, the electron and hole mobilities were 1 and 0.01 $cm^2/(V \cdot s)$ respectively. All device simulations were performed at room temperature of 300K and were illuminated by the AM1.5 power spectrum of $100mw/cm^2$ from the top surface.

The illuminated current density (J) is plotted as a function of the cell voltage in Fig. 5. We note that the {110} GBE devices $(B-D)$ have slightly higher short circuit current density (J_{SC}) compared to c-Si. This is because the {110} GBE silicon has significantly higher absorption coefficients than c-Si for wavelengths in the visible region - the 16% increase in absorbed photons more than compensates for the decrease in free-carrier generation from the larger band gap, yielding a net 1% increase in current generation by device (B), relative to c-Si (A). The integrated generation rate over the entire 2-D surface showed that the total number of charge carriers generated upon optical excitation is higher in the {110} GB devices compared to that of c-Si. Hence, {110} GBs show marginally higher short circuit current than c-Si for the device thicknesses that we have studied, but with this benefit increasing as

1 2 3 4 5 6 7 8 9 10 11 12 13 14 15 16 17 18 19 20 21 22 23 24 25 26 27 28 29 30 31 32 33 34 35 36 37 38 39 40 41 42 43 44 45 46 47 48 49 50 51 52 53 54 55 56 57 58 59 60

devices are made thinner. The computed peak J_{SC} for a-Si:H is $16.9 mA/cm^2$, considerably less than both the c-Si device, as well as our GB structures, due to the substantially degraded carrier transport in the fully amorphous material.

The most significant result of the GBE device simulations is the remarkable improvement in V_{OC} accompanying the improved absorption. Our results show that the higher band gap of {110} GBs significantly increases the open circuit voltage (V_{OC}), which, when combined with the significantly increased absorption offsetting the decreased current production from the band gap increase, results in up to a 46% (relative) improvement in energy conversion efficiency in GBE devices over c-Si. This increased voltage can be understood by considering the dependence of V_{OC} on carrier concentrations:

$$V_{oc} = \frac{k_B T}{q} ln \left[\frac{(N_A + \Delta p)\Delta n}{n_i^2} \right] \quad (2)$$

where k_B is the Boltzmann constant, T is the temperature, q is the electron charge, N_A is the doping concentration, $\Delta n = \Delta p$ is the excess carrier concentration and n_i is the intrinsic carrier concentration.[59] The term $k_B T/q$, called the thermal voltage, is equal to $0.026V$. Since we use the same doping concentration in all our devices, n_i directly governs the V_{OC} of the device. As the carrier concentration in an intrinsic semiconductor decreases exponentially with increased band gap of the material at a given temperature, an increase in band gap can be correlated to the observed increases in V_{OC}.

Furthermore, from the Shockley-Queisser model, the temperature dependence of V_{OC} can be directly related to E_g by,

$$V_{oc} = E_g/q - CT \quad (3)$$

where, C is the temperature coefficient representing dark current characteristics of a solar

cell device. Taking $C = 2 \times 10^{-3} V/K$ for c-Si,[2,60] and since the presence of {110} GBs have no significant impact on the charge mobilities, we can calculate V_{OC} to be $0.57V$ $0.78V$, $0.75V$ and $0.73V$ at room temperature for devices $(A \rightarrow D)$, respectively. As expected, these values are consistent with the values obtained from the $J - V$ curve, which is further confirmed by the higher $V_{oc} = 0.96V$ of the fully amorphous device (E), which has a band gap of 1.65eV. The key results from our device model are presented in table 1.

One major factor that can influence the carrier mobilities in these devices is the segregation of impurities and point defects at the GB. In order to understand how the device performance is affected by changes in carrier mobilities, we performed device modeling for a range of electron and hole mobilities for the GB spacing 3.1nm. Earlier, Seager had shown that in polysilicon with random GBs, the resistivity values increased by a factor of 2 to 3 compared to c-Si in the doping density limits that we have studied here.[61] Hence, in the device models, we used electron mobilities in the range 1450 cm^2/Vs (c-Si limit) to 483 cm^2/Vs and hole mobilities in the range 500 cm^2/Vs (c-Si limit) to 167 cm^2/Vs for all the three principal directions. We also decreased the carrier lifetimes to account for increased recombination in presence of point defects. A wide range of carrier lifetime anywhere between 0.1 μs to 1.0 μs has been reported in the literature.[62,63] We however chose the lowest value of 0.1 μs for electron and hole lifetimes for the GB structures, which is two orders smaller than that in c-Si (10 μs). Even with this more realistic and stringent model, we find that the efficiencies of GBE devices are still much higher than the c-Si device (A) (Table 2).

Table 2: Results from the solar cell device models for devices with GB spacing 3.1nm under AM1.5 illumination for different carrier mobilities and carrier lifetime of 0.1 μs; $\mu_e(Si) = 1450\ cm^2/Vs$ and $\mu_h(Si) = 500\ cm^2/Vs$ are the mobilities in c-Si

Device	μ_e	μ_h	$\mathbf{J_{SC}}$ **(mA/cm²)**	$\mathbf{V_{OC}}$ **(mV)**	**Fill factor (FF)**	**Efficiency** (η)
F	$\mu_e(Si)$	$\mu_h(Si)$	29.09	775	0.85	19.38%
G	$\mu_e(Si) * 2/3$	$\mu_h(Si) * 2/3$	28.36	777	0.85	18.95%
H	$\mu_e(Si) * 1/2$	$\mu_h(Si) * 1.2$	27.66	779	0.85	18.53%
I	$\mu_e(Si) * 2/5$	$\mu_h(Si) * 2/5$	26.99	780	0.85	18.10%
J	$\mu_e(Si) * 1/3$	$\mu_h(Si) * 1/3$	26.36	782	0.85	17.73%

1
2
3
4
5
6
7
8
9
10
11
12
13
14
15
16
17
18
19
20
21
22
23
24
25
26
27
28
29
30
31
32
33
34
35
36
37
38
39
40
41
42
43
44
45
46
47
48
49
50
51
52
53
54
55
56
57
58
59
60

While the GBE devices studied here represent highly dense configurations of GBs (as using DFT to compute optical and electronic properties for GB spacings >10nm become computationally demanding), by performing a second-order polynomial extrapolation of the data (columns 2 and 6) in table 1, we calculate that it is still possible to obtain an approximately 10% relative improvement in V_{OC} and efficiency over c-Si in GBE structures with spacings as far as 25nm apart. This indicates that experimentally-feasible structures could not only be within reach, but hold promise of further efficiency enhancements as the ability to increase the density of the engineered GBs improves.

Conclusions

We have shown that by understanding the role of GBs on the optical and electronic properties of c-Si, it is possible to design novel nanostructured material architectures with improved photovoltaic properties. We find that the {111} twin boundaries have minimal atomic rearrangement at the interface, with changes to the electronic structure being relatively insignificant, while the {112} GBs are associated with bonding defects which lead to metallic behavior. The {110} GBs, however, possess an increased band gap relative to c-Si, which alone is shown to yield relative V_{OC} improvements of 28% to 37% over c-Si, for GB spacings of 6.2 to 3.1nm, respectively (Table 1).

For the {110} GB, we additionally find a significant improvement in the optical absorption over much of the visible spectrum, without degradation in the overall electronic conductivity relative to c-Si. The absorption of the GBE material is shown to yield relative J_{SC} improvements of 1.4% to 1.9% over c-Si even after compensating for the decreased accessible energy range due to the increased band gap, again for the respective GB spacings of 6.2 to 3.1nm, in $5\mu m$ thick cells. As the push toward ultra-thin, kerfless wafer processing allows c-Si substrates to be made continually thinner, this enhanced absorption becomes increasingly advantageous.

By combining these electronic structure calculations into FEM device models, we have shown that PV devices containing optimally-spaced 3.1nm GBE configurations could potentially benefit from efficiency improvements as high as 46% over comparable thin-film c-Si devices. At reduced GB densities (20nm spacing) and for thick devices ($\sim$ 100% absorption above E_g), we still predict 4% relative efficiency improvements over c-Si, due to the increased band gap. This combination of the enhanced absorption for thin materials, as well as enhanced band gap for dense GB arrangements, could make these GBE structures attractive candidates for the design of future novel and efficient solar cells.

Author Information

Corresponding Author

*E-mail: jcg@mit.edu.

Notes:

The authors declare no competing financial interest.

Supporting Information Available

Details of methodology, atomic structure, zone folding in extended silicon supercells, GGA *vs.* meta-GGA band structures, valence and conduction band charge densities for the GB structures, cohesive energy, effect of GB spacing on optical absorption, absorptive power of GB materials compared to c-Si and a-Si:H, computed electronic conductivities of {110} GB as a function of GB spacing and electronic conductivity of c-Si under strain are presented in the supporting information. This material is available free of charge via the Internet at `http://pubs.acs.org/`.

Acknowledgement

This work was supported by grants from King Fahd University of Petroleum and Minerals (KFUPM) in Dhahran, Saudi Arabia under Project No. R1-CE-08. The authors acknowledge Teragrid for computational resources, supported by the National Science Foundation under Grants TG-DMR090027 and TG-DMR110027. RR acknowledges Dr. Joo-Hyoung Lee, GIST, Korea and Dr. Engin Durgun, Bilkent University, Turkey, for their help during this project.

References

(1) *Greentech Media Research, PV News* **2012**, *31*, 1–28.

(2) Shockley, W.; Queisser, H. J. *J. Appl. Phys.* **1961**, *32*, 510–519.

(3) Liang, J.; Schiff, E. A.; Guha, S.; Yan, B.; Yang, J. *Appl. Phys. Lett.* **2006**, *88*, 063512.

(4) Staebler, D. L.; Wronski, C. R. *Appl. Phys. Lett.* **1977**, *31*, 292–294.

(5) Street, R. *Hydrogenated Amorphous Silicon*; Cambridge University Press, 1991; pp 390–391.

(6) Chen, H.; Gullanar, M.; Shen, W. *J. Cryst. Growth* **2004**, *260*, 91 – 101.

(7) Reynolds, S. *J. Optoelectron. Adv. Mater.* **2009**, *11*, 1086–1092.

(8) NREL Efficiency Chart. `http://www.nrel.gov/ncpv/images/efficiency_chart.jpg`.

(9) Bruhne, K.; Schubert, M.; Kohler, C.; Werner, J. *Thin Solid Films* **2001**, *395*, 163 – 168.

(10) Yue, G.; Yan, B.; Ganguly, G.; Yang, J.; Guha, S.; Teplin, C. W. *Appl. Phys. Lett.* **2006**, *88*, 263507.

(11) Pearce, J. M.; Podraza, N.; Collins, R. W.; Al-Jassim, M. M.; Jones, K. M.; Deng, J.; Wronski, C. R. *J. Appl. Phys.* **2007**, *101*, 114301.

(12) Kohyama, M.; Yamamoto, R. *Phys. Rev. B* **1994**, *49*, 17102–17117.

(13) Morris, J. R.; Fu, C. L.; Ho, K. M. *Phys. Rev. B* **1996**, *54*, 132–138.

(14) Watanabe, T.; Kido, K.; Tsurekawa, S.; Kawahara, K. *Mater. Sci. For.* **2007**, *558-559*, 843–850.

(15) Watanabe, T.; Tsurekawa, S.; Zhao, X.; Zuo, L. In *Microstructure and Texture in Steels*; Haldar, A., Suwas, S., Bhattacharjee, D., Eds.; Springer London, 2009; pp 43–82.

(16) Jeon, J.-H.; Park, K.-C.; Lee, M.-C.; Han, M.-K. *J. Non-Cryst. Solids* **2000**, *266-269*, 645 – 649.

(17) Huang, W. L.; Ge, W.; Li, C.; Hou, C.; Wang, X.; He, X. *Comput. Mater. Sci.* **2012**, *58*, 38 – 44.

(18) Suvitha, A.; Venkataramanan, N. S.; Sahara, R.; Mizuseki, H.; Kawazoe, Y. *Jpn. J. Appl. Phys.* **2010**, *49*, 04DP02.

(19) Feng, C. B.; Nie, J. L.; Zu, X. T.; Al-Jassim, M. M.; Yan, Y. *J. Appl. Phys.* **2009**, *106*, 113506.

(20) Sawada, H.; Ichinose, H.; Kohyama, M. *J. Phys.: Condens. Matter* **2007**, *19*, 026223.

(21) Yan, Y.; Jones, K.; Jiang, C.; Wu, X.; Noufi, R.; Al-Jassim, M. *Phys. B (Amsterdam, Neth.)* **2007**, *401-402*, 25 – 32.

(22) Wang, Z.-J.; Tsurekawa, S.; Ikeda, K.; Sekiguchi, T.; Watanabe, T. *Interface Sci.* **1999**, *7*, 197–205.

(23) Ogawa, H. *Mater. Trans.* **2006**, *47*, 2706–2710.

1
2
3
4
5
6
7
8
9
10
11
12
13
14
15
16
17
18
19
20
21
22
23
24
25
26
27
28
29
30
31
32
33
34
35
36
37
38
39
40
41
42
43
44
45
46
47
48
49
50
51
52
53
54
55
56
57
58
59
60

(24) Kresse, G.; Furthmuller, J. *Comput. Mater. Sci.* **1996**, *6*, 15 – 50.

(25) Blöchl, P. E. *Phys. Rev. B* **1994**, *50*, 17953–17979.

(26) Kresse, G.; Joubert, D. *Phys. Rev. B* **1999**, *59*, 1758–1775.

(27) Perdew, J. P.; Burke, K.; Ernzerhof, M. *Phys. Rev. Lett.* **1996**, *77*, 3865–3868.

(28) Perdew, J. P.; Burke, K.; Ernzerhof, M. *Phys. Rev. Lett.* **1997**, *78*, 1396–1396.

(29) Vojta, T.; Mertig, I.; Zeller, R. *Phys. Rev. B* **1992**, *46*, 15761–15766.

(30) Thonhauser, T.; Scheidemantel, T. J.; Sofo, J. O. *Appl. Phys. Lett.* **2004**, *8*, 588–590.

(31) Yang, J.; Li, H.; Wu, T.; Zhang, W.; Chen, L.; Yang, J. *Adv. Funct. Mater.* **2008**, *18*, 2880–2888.

(32) Singh, D. J. *Phys. Rev. B* **2010**, *81*, 195217.

(33) May, A. F.; Singh, D. J.; Snyder, G. J. *Phys. Rev. B* **2009**, *79*, 153101.

(34) Lee, M.-S.; Poudeu, F. P.; Mahanti, S. D. *Phys. Rev. B* **2011**, *83*, 085204.

(35) Ashcroft, N. W.; Mermin, D. N. *Solid State Physics*; 2009; pp 213–229.

(36) Gaymann, A.; Geserich, H. P.; Löhneysen, H. v. *Phys. Rev. B* **1995**, *52*, 16486–16493.

(37) Weber, L.; Gmelin, E. *Appl. Phys. A* **1991**, *53*, 136–140.

(38) Sakaguchi, N.; Ichinose, H.; Watanabe, S. *Mater. Trans.* **2007**, *48*, 2585–2589.

(39) Sakaguchi, N.; Miyake, M.; Watanabe, S.; Takahashi, H. *Mater. Trans.* **2011**, *52*, 276–279.

(40) Kholod, A.; Borisenko, V.; Saúl, A.; d'Avitaya, F. A.; Fuhr, J. *Opt. Mater.* **2001**, *17*, 61 – 63.

1
2
3
4
5
6
7
8
9
10
11
12
13
14
15
16
17
18
19
20
21
22
23
24
25
26
27
28
29
30
31
32
33
34
35
36
37
38
39
40
41
42
43
44
45
46
47
48
49
50
51
52
53
54
55
56
57
58
59
60

(41) Ke, S.-h.; Zhang, K.-m.; Xie, X.-d. *Phys. Rev. B* **1997**, *55*, 5124–5128.

(42) Zhao, X.; Wei, C. M.; Yang, L.; Chou, M. Y. *Phys. Rev. Lett.* **2004**, *92*, 236805.

(43) Ng, M.-F.; Sullivan, M. B.; Tong, S. W.; Wu, P. *Nano Lett.* **2011**, *11*, 4794–4799.

(44) Zhang, L.; d'Avezac, M.; Luo, J.-W.; Zunger, A. *Nano Lett.* **2012**, *12*, 984–991.

(45) Boykin, T. B.; Klimeck, G. *Phys. Rev. B* **2005**, *71*, 115215.

(46) Ku, W.; Berlijn, T.; Lee, C.-C. *Phys. Rev. Lett.* **2010**, *104*, 216401.

(47) Ferraro, E.; Hogan, C.; Palummo, M.; Del Sole, R. *Phys. Status Solidi B* **2012**, *249*, 1148–1154.

(48) Malone, B. D.; Sau, J. D.; Cohen, M. L. *Phys. Rev. B* **2008**, *78*, 035210.

(49) Malone, B. D.; Sau, J. D.; Cohen, M. L. *Phys. Rev. B* **2008**, *78*, 161202.

(50) Tran, F.; Blaha, P. *Phys. Rev. Lett.* **2009**, *102*, 226401.

(51) Dudeck, K. J.; Walters, W. D.; Knights, A. P.; Coleman, P. G. *J. Phys. D* **2008**, *41*, 055102.

(52) Farid, B.; Godby, R. W. *Phys. Rev. B* **1991**, *43*, 14248–14250.

(53) Johlin, E.; Wagner, L. K.; Buonassisi, T.; Grossman, J. C. *Phys. Rev. Lett.* **2013**, *110*, 146805.

(54) Weber, L.; Gmelin, E. *Appl. Phys. A* **1991**, *53*, 136–140.

(55) Hinsche, N.; Mertig, I.; Zahn, P. *J. Phys.: Cond. Mat.* **2011**, *23*, 295502.

(56) Visoly-Fisher, I.; Cohen, S.; Gartsman, K.; Ruzin, A.; Cahen, D. *Adv. Funct. Mater.* **2006**, *16*, 649–660.

1
2
3
4
5
6
7
8
9
10
11
12
13
14
15
16
17
18
19
20
21
22
23
24
25
26
27
28
29
30
31
32
33
34
35
36
37
38
39
40
41
42
43
44
45
46
47
48
49
50
51
52
53
54
55
56
57
58
59
60

(57) Saha, S.; Hilali, M. M.; Onyegam, E. U.; Sarkar, D.; Jawarani, D.; Rao, R. A.; Mathew, L.; Smith, R. S.; Xu, D.; Das, U. K.; Sopori, B.; Banerjee, S. K. *Appl. Phys. Lett.* **2013**, *102*, 163904.

(58) Schropp, R.; Zeman, M. *Amorphous and microcrystalline silicon solar cells: Modeling, Materials and Device Technology*; Kluwer, 1998; pp 29–30.

(59) Sinton, R. A.; Cuevas, A. *Appl. Phys. Lett.* **1996**, *69*, 2510–2512.

(60) Tayagaki, T.; Hoshi, Y.; Usami, N. *Sci. Rep.* **2013**, *3*, 2703.

(61) Seager, C. H. *Annu. Rev. Mater. Sci.* **1985**, *15*, 271–302.

(62) Metzger, W. K. *Sol. Energy Mater. Sol. Cells* **2008**, *92*, 1123–1135.

(63) Sakata, I.; Hayashi, Y.; ichi Ishii, K.; Takahashi, T.; Yamanaka, M. *Jpn. J. Appl. Phys.* **1986**, *25*, L328–L330.

Graphical TOC Entry

	c-Si	a-Si:H	GBE-Si
Band Gap (eV)	1.17	1.68	1.38
Optical Absorption	Poor	Good	Good
Mobility	Good	Poor	Good